Research article

Jan Fait*, Marián Varga, Karel Hruška, Alexander Kromka, Bohuslav Rezek and Lukáš Ondič

# Spectral tuning of diamond photonic crystal slabs by deposition of a thin layer with silicon vacancy centers

https://doi.org/10.1515/nanoph-2021-0369
Received July 12, 2021; accepted September 2, 2021;
published online September 17, 2021

**Abstract:** The controlled extraction of light from diamond optical color centers is essential for their practical prospective applications as single photon sources in quantum communications and as biomedical sensors in biosensing. Photonic crystal (PhC) structures can be employed to enhance the collection efficiency from these centers by directing the extracted light towards the detector. However, PhCs must be fabricated with nanoscale precision, which is extremely challenging to achieve for current materials and nanostructuring technologies. Imperfections inherently lead to spectral mismatch of the extraction (leaky) modes with color center emission lines. Here, we demonstrate a new and simple two-step method for fabricating diamond PhC slabs with leaky modes overlapping the emission line of the silicon vacancy (SiV) centers. In the first step, the PhC structure with leaky modes blue shifted from the SiV emission line is fabricated in a nanocrystalline diamond without SiV centers. A thin layer of SiV-rich diamond is then deposited over the PhC slab so that the spectral position of the PhC leaky modes is adjusted to the emission line of the SiV centers, thereby avoiding the need for nanoscale precision of the structuring method. An intensity enhancement of the zero-phonon line of the SiV centers by a factor of nine is achieved. The color centers in the thin surface layer are beneficial for sensing applications and their properties can also be further controlled by the diamond surface chemistry. The demonstrated PhC tuning method can also be easily adapted to other optical centers and photonic structures of different types in diamond and other materials.

**Keywords:** leaky modes; nanocrystalline diamond; photonic crystal slab; silicon vacancy; spectral tuning.

## 1 Introduction

Diamond color centers are light-emitting defects of diamond lattice [1] with potential applications in quantum information processing [2, 3], magnetometry [4, 5], and sensing [6, 7]. One of the most well-known color centers in diamond is the silicon vacancy (SiV) center [2, 8], the intensity of which depends on the surrounding environment, such as the surface termination [9]. The intensity of the photoluminescence (PL) of SiV centers and their PL decay dynamics can serve as measures of changes in the surroundings. Together with the chemical and physical stability of diamond, the sensitivity to the changes in the surrounding can be employed for gas and bio sensing. In our previous works, an ensemble of SiV centers was distributed homogeneously in a diamond layer [10, 11]. However, for sensing applications, the placement of the color centers near the diamond surface is essential as the centers lying deep inside the material are insulated from the surface changes and only contribute to the idle PL background. On the other hand, the PL intensity of a thin layer with SiV centers is very low [9] and requires sophisticated detection techniques. In order to exploit this potential application of SiV centers, the first step is to develop an approach that will enable the fabrication of suitable structures for sensing experiments.

The combination of photonic structures with diamond can improve the performance of devices based on the PL of diamond color centers, which all require high emission rate and collection efficiency of light. Photonic crystal

***Corresponding author: Jan Fait**, Institute of Physics CAS, Cukrovarnická 10, 16200 Prague, Czech Republic, E-mail: fait@fzu.cz. https://orcid.org/0000-0003-3084-3220
**Marián Varga,** Institute of Physics CAS, Cukrovarnická 10, 16200 Prague, Czech Republic; and Institute of Electrical Engineering, Slovak Academy of Sciences, Dúbravská cesta 9, 841 04 Bratislava, Slovak Republic, E-mail: varga@fzu.cz
**Karel Hruška, Alexander Kromka and Lukáš Ondič,** Institute of Physics CAS, Cukrovarnická 10, 16200 Prague, Czech Republic, E-mail: hruskak@fzu.cz (K. Hruška), kromka@fzu.cz (A. Kromka), ondic@fzu.cz (L. Ondič)
**Bohuslav Rezek,** Faculty of Electrical Engineering, Czech Technical University in Prague, Technická 2, 16627 Prague, Czech Republic, E-mail: rezekboh@fel.cvut.cz

(PhC) cavities [12–14] or ring resonators [15] enable the emission rate of color centers to be locally increased due to the Purcell effect [16]. Nevertheless, a significant portion of radiative emission is directed at azimuthal angles larger than 50° [17–19] and thus must be collected with large numerical aperture (NA) objectives. PhC cavities are especially suitable for applications in single-center-based quantum photonics. Slotted PhC cavities, in which the cavity mode is located dominantly in air, have also been employed for sensing applications [6, 20]. However, sophisticated optical components are required for coupling/outcoupling light into such optical components and the size of the active area, which is sensitive to the change in the surroundings, is dictated by the relatively small dimensions of the cavity (a few micrometers).

In contrast, PhC slabs, formed when a thin layer of material is patterned with two-dimensional (2D) periodicity, offer a much larger active area (from $mm^2$ up to $cm^2$) that can improve the PL collection efficiency [11, 21]. The guided modes supported by planar layers are coupled with the radiation modes via the Bragg diffraction phenomenon [22], which markedly increases the extracted PL signal intensity. Such modes are referred to as leaky modes in PhC slabs. Leaky modes can also be employed in the spatially resolved sensing of the environment, because the resonance condition depends on the refractive index at a specific location of the device [23, 24]. We have already shown that PhC slabs can be fabricated in nanocrystalline diamond (NCD) layers, while retaining excellent performance for light extraction [11], and that the PhC slabs can be engineered to efficiently extract the PL of SiV centers [10]. The advantage of NCD over single-crystal diamond is its cost-effective deposition on various substrate materials using chemical vapor deposition (CVD) [25, 26]. Furthermore, optical centers, such as SiV, nitrogen vacancy (NV) and germanium vacancy (GeV) centers can be incorporated at high densities during the growth, which makes NCD a potential material for optical center-based sensing.

In contrast, the photonic structures fabricated on the NCD possess structural imperfections due to its grain-like structure, which makes it impossible to fabricate structures that exactly match the requirements of the simulation. Nevertheless, the same issue also holds for single-crystal diamond-based photonic structures, where deviations, such as the non-verticality of sidewalls or nanometer-scale variance of dimensions, were observed [27]. Therefore, post-fabrication tuning is often required to achieve spectral overlap between the photonic modes and narrow emission lines of quantum dots or colors centers. In general, the tuning mechanism can be based on material removal using an electron beam [28], wet etching [29] or surface oxidation [27, 30], material addition using nanofluidic channels [31], or thermooptic [32, 33] and photochromic tuning [34, 35]. In diamond, surface oxidation [27] and the condensation of gases at cryogenic temperatures [36, 37] were demonstrated to finely tune the spectral position of photonic modes in cavities. The disadvantage of these methods lies in the possible surface damage in the former case and the need for a cryogenic chamber in the latter case, which is not suitable for sensing experiments. None of these approaches enable the creation of a thin layer with the color centers required for sensing.

In this contribution, we present a strategy for the postfabrication spectral tuning of the leaky modes of PhC slabs in diamond with the potential to tune the spectral position of modes with nanometer scale precision. The tuning mechanism is based on the controlled addition of a new diamond layer that increases the PhC slab thickness and red shifts the leaky modes to the desired spectral position. We demonstrate the mechanism by altering the dimensions of a pre-patterned polycrystalline diamond layer via deposition of a second diamond tuning layer in order to shift the position of leaky modes to the zero-phonon line (ZPL) of SiV centers (738 nm). Simultaneously, SiV centers are incorporated into this tuning layer to yield SiV centers not in the whole volume of the diamond material but located only near the diamond surface. We show that such PhC slabs enable the efficient extraction of the PL from the near-surface-located SiV centers into the surroundings via coupling to the leaky modes. We also show that the PL intensity of the SiV centers can be improved by altering the surface properties through oxygen plasma treatment. These photonic structures present an ideal configuration for sensing applications, where both the nearby surface deposited color centers and the spectral characteristics of the leaky modes are strongly affected by the changes in the surrounding environment.

## 2 Materials and methods

The NCD layers were grown on a quartz substrate that was first ultrasonically cleaned in acetone and isopropyl alcohol and rinsed in deionized water. After the cleaning, the quartz substrate was seeded by applying ultrasonic agitation in an aqueous nanodiamond colloidal dispersion (NanoAmando colloid, median nanodiamond size of 4.8 ± 0.6 nm) diluted by deionized water (1:40 v:v).

For the diamond growth, two different CVD reactors were employed: (i) A linear antenna microwave (MW) plasma system (Roth & Rau AK 400) equipped with two linear antennas working in a pulsed regime and (ii) a focused MW plasma reactor (Aixtron P6) using an ellipsoidal cavity resonator [38]. The parameters used for the diamond deposition in the linear antenna MW plasma system were a deposition

time ($t$) of 19 h, a pressure ($p$) of 10 Pa, a gas flow of $H_2$ equal to 200 sccm, a gas flow of $CH_4$ equal to 5 sccm, a gas flow of $CO_2$ equal to 20 sccm, a MW source power ($P$) of 2 × 1.7 kW and a sample surface temperature ($T$) of ≈540 °C. The thickness of the layer was ≈160 nm, as measured by reflectance interferometry. This deposition system is suitable for growing thin diamond layers without the SiV center PL even on substrate materials that contain Si atoms [39]. We used this deposition system for growing the SiV-free diamond layers used for the subsequent nanopatterning. Scanning electron microscopy (SEM) image of the planar layer and its PL spectrum are available in the Supplementary material (Figures S2 and S3(a), respectively).

The top part of the diamond layer was then patterned into the periodically ordered columns using electron beam lithography (EBL) and reactive ion etching (RIE) to yield a PhC slab. An electron sensitive polymer (poly(methyl methacrylate), thickness of ≈100 nm) was first patterned by EBL. Next, the gold (thickness of ≈70 nm) was evaporated and the mask was created using a lift-off process. Not-covered parts of the sample were partially etched with capacitively coupled $O_2/CF_4$ plasma RIE. Finally, the metal mask was removed by wet etching. The total area of the PhC structure on the sample was 1 $mm^2$.

After the optical characterization of the fabricated PhC slab and the non-patterned (reference) layer, the second layer of NCD was grown in the focused MW plasma reactor with a $t$ of 15 min, a $p$ of 6 kPa, a gas flow of $H_2$ equal to 300 sccm, a gas flow of $CH_4$ equal to 3 sccm, a $P$ of 3 kW and $T$ of ≈820 °C. Pieces of common intrinsic Si wafer, which were placed into the vicinity of the sample, served as a source of Si atoms for the formation of SiV centers as they were partially etched by plasma during the diamond deposition. The PhC dimensions before and after the second deposition are specified in Figure 1.

The growth rate for the deposition of the tuning layer was ≈4 nm/min. This fast growth rate is an inherent property of the deposition system used for the deposition of diamond layers with SiV centers. In order to achieve nanoscale precision, a deposition chamber with a

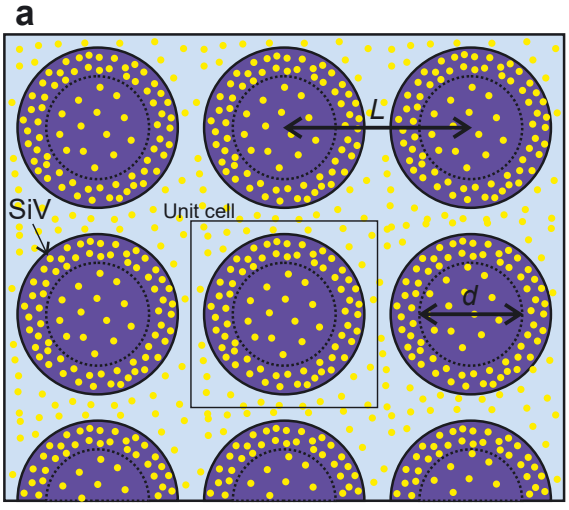


| Parameter | Original | + Tuning |
|---|---|---|
| $L$ | 390 nm | 390 nm |
| $d$ | 215 nm | 335 nm |
| $t_{PhC}$ | 105 nm | 105 nm |
| $t_W$ | 55 nm | 115 nm |
| $t_{ref} \approx t$ | 160 nm | 220 nm |

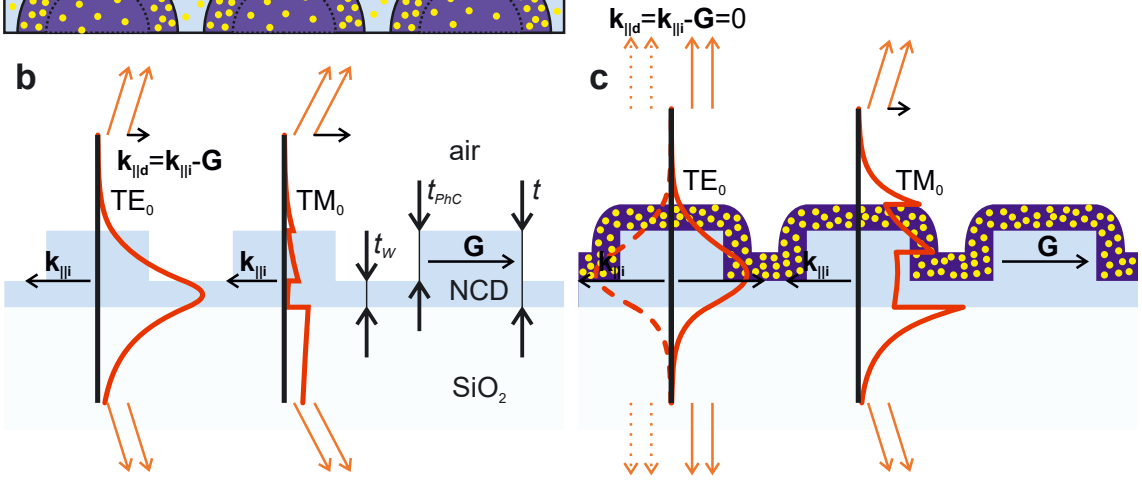


**Figure 1:** (a) Schematic overview of the photonic crystal (PhC) structure composed of periodically-ordered columns investigated in this study. The SiV-rich (yellow dots) tuning layer is also depicted. Dotted circles denote the dimensions of the original diamond structure without the SiV-rich layer. The table summarizes the dimensions of the PhC slab: lattice constant ($L$), column diameter ($d$), thickness of PhC layer ($t_{PhC}$), thickness of waveguiding layer ($t_W$) and total thickness ($t$). The estimated uncertainty is 5–10 nm. (b) Cross section of the original PhC slab with the scheme of the Bragg diffraction of the fundamental $TE_0$ and $TM_0$ modes on a thin dielectric layer for a given wavelength. (c) To change the Bragg diffraction condition and the propagation of light after extraction, the tuning layer (denoted by the dark blue color with yellow dots) can be deposited on top, which increases the propagation constant of the mode $\mathbf{k}_{||i}$ (see text). The spatial profile of the electric field of the modes was computed by an online mode solver [44], where the constant effective refractive index of the top PhC layer was used.

slower growth rate must be used. For instance, the growth rate of the original layer was ≈8 nm/h and offers higher control over the thickness. However, this apparatus does not enable the color centers to be embedded during the growth. In contrast, the controlled growth of ≈1 nm layers with optical centers is possible using deposition chambers of other manufacturers, as demonstrated, for example, with NV centers in Ref. [40]. The other possibility for achieving nanoscale growth precision is to use silane for Si doping [41]. Using silane as a source of Si atoms instead of the Si wafers enables a decrease in the growth rate.

The surface morphology of the samples was investigated by SEM (Tescan, MAIA3) in a standard configuration for secondary electron imaging. The thickness and refractive index of the diamond film (both before and after etching) were measured by reflectance interferometry and evaluated by commercially available Film Wizard software (SCI).

A Renishaw in Via Reflex system was used for the PL measurements. Multiple objectives (5× with NA 0.12, 20× with NA 0.4, 50× with NA 0.5 and 100× with NA 0.9) were used for the collection of signals. The maximal collection angle depends on the NA of the objective. Furthermore, the size of the probed area depends on the NA and is of the order of square micrometers for all objectives. This may limit the portion of collected leaky modes as the propagation length in the layer also lies in this range. The depth of focus is larger than the thickness of the samples for all objectives. A He–Cd laser (442 nm) was used for the excitation of the PL in both cases. The spectra were corrected for the spectral response of the detection system.

The angle-resolved transmission and PL measurements, which allow us to map the spectral position of leaky modes for different angles of incidence, were realized in the setup shown in the Supplementary material (Fig. S8). A collimated white light was transmitted through the sample and detected using an optical fiber connected to a spectrometer with an intensified CCD camera (Andor) at the output. The sample was rotated around the axis perpendicular to one of the main symmetry directions (Γ–*X*) of the PhC. For the simulation of transmission through the sample, the rigorous coupled-wave analysis (RCWA) method (RSoft DiffractMod) was used. The same detection as for transmission measurements was used also for the PL measurements, while the focused laser beam (442 nm) was used for the excitation of the PL. For this experiment, the sample was stationary and the fiber was rotated around the sample along the Γ–*X* direction.

## 3 Results and discussion

The majority of light emitted by the emitters in thin NCD layers is coupled to the guided modes. Part of this light is recovered via scattering on material inhomogeneities (grain boundaries) and on the inherently rough surface. The rest is absorbed on material defects in NCD before reaching the edge of the sample. Nevertheless, rough structures produce light with a Lambertian radiation pattern [42] and do not allow for control of the propagation of light after extraction. Encapsulation of the layer [43] is not applicable for sensors that require direct access to the material.

In the PhC slabs, light is diffracted via Bragg diffraction and its propagation constant is changed in a defined way:

$$\mathbf{k}_{\|\mathbf{d}} = \mathbf{k}_{\|\mathbf{i}} + m\mathbf{G} \quad (1)$$

where $\mathbf{k}_{\|\mathbf{i}}$ and $\mathbf{k}_{\|\mathbf{d}}$ are the propagation constant (in-plane wavevector) before and after the diffraction event, respectively, $m$ is an integer, and $\mathbf{G}$ is the reciprocal lattice vector. When $|\mathbf{k}_{\|\mathbf{d}}| < k_0 = \frac{2\pi}{\lambda_0}$, where $k_0$ and $\lambda_0$ are the wavevector and vacuum wavelength of light, respectively, the $z$-component of the $k$-vector becomes real $k_z = \sqrt{k_0^2 - k_{\|d}^2}$. The photonic modes of the PhC slab can then couple to radiative modes and escape from the layer, as depicted in Figure 1 for the fundamental transverse-electric ($TE_0$) and transverse magnetic ($TM_0$) modes, respectively. These modes are known as leaky modes or guided resonances.

In order to reach the spectral overlap of leaky modes with the spectrum of the emitters, the dimensions of PhC slabs must be simulated in advance. The fabrication of structures that exactly match the simulation outputs is almost impossible and the deviations of the real sample dimensions from the simulation also lead to the spectral shift of the modes. Figure 2 shows the strong dependence of the spectral position of the vertically-extracted $TE_0$ leaky mode on the parameters of the PhC structures computed using the RCWA technique. For instance, the refractive index of the NCD layers, which deviates from the values for single-crystal diamond (see Supplementary material) by only ≈3%, causes a spectral shift of more than 25 nm. In practice, the situation is even more complex because the refractive index depends on the deposition parameters of the CVD process and may slightly differ for individual samples. The deviation of 5 nm in etching depth ($t_w$ and $t_{PhC}$) with respect to the simulation leads to a spectral shift of the $TE_0$ mode of ≈5 nm. The deviation of 5 nm in the column diameter ($d$) leads to a spectral shift of ≈1 nm. Moreover, the shape of the columns may differ due to different etching rates near the masked regions, which cannot be reliably included in the simulation. All these factors may lead to significant spectral shifts of the modes in the fabricated structures with respect to the designed structures.

To overcome these inherent difficulties regarding the PhC slab design and fabrication, we employed the following procedure: 1) PhC slabs were designed to support leaky modes that are blue shifted from the required spectral position. 2) After the fabrication, the PhC slabs were characterized and the spectral positions of the leaky modes were measured. 3) A new tuning layer was grown on top of the PhC slab, which tunes the leaky modes to the required spectral position. Note that fine-tuning may be achieved by using multiple repetition of the steps 2) and 3) with nanometer thin layers. This approach avoids the change in the lattice constant that is not possible during post-fabrication. Instead, the propagation constant of the mode is increased via an increase in the effective refractive index:

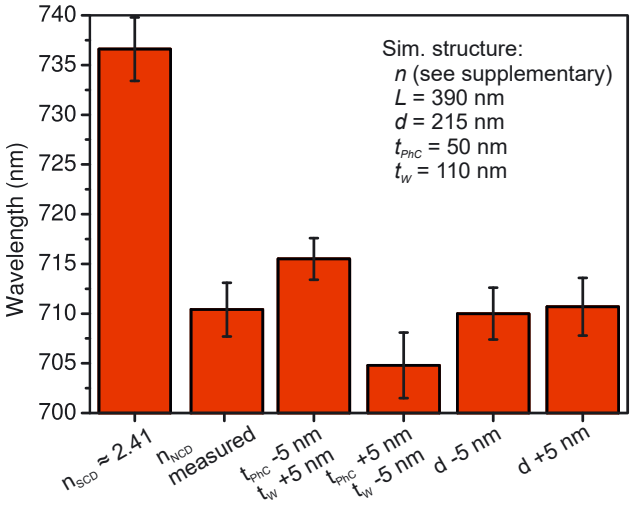


**Figure 2:** Simulated spectral position of the $TE_0$ leaky mode for normal incidence and its dependence on the refractive index of the layer (refractive index of single-crystal diamond [SCD] and nanocrystalline diamond [NCD], for details on the refractive index, see Figure S1 in the Supplementary material), on the depth of etching (shallower etching increases $t_w$ and reduces $t_{PhC}$) and on the diameter of columns ($d$). The error bars correspond to the spectral full width at half maximum (FWHM) of the leaky modes.

$$N_{\text{eff}} = \frac{|\mathbf{k}_{||}|}{k_0} < n_{\text{mat}} \tag{2}$$

as a larger portion of the mode propagates in the material with a high refractive index $n_{\text{mat}}$ (as seen from comparing the spatial profiles of the $TE_0$ and $TM_0$ modes of the original and overgrown PhC structures in Figure 1(b) and (c)).

Moreover, our method allows us to alter the material properties, such as the SiV center concentration, $sp^2$ carbon content, grain size and roughness, in the tuning and original layers or even in multiple individual tuning layers, which provides an opportunity to tune their properties based on the future application. Figure 1(c) schematically depicts the cross section of the PhC slab with the new layer that was intentionally deposited in the particular CVD apparatus to enable the incorporation of SiV centers during the growth. The thickness of the perturbed layer $t_{\text{PhC}}$ remains unchanged when the growth is isotropic (approximately true for NCD), while the waveguide thickness ($t_w$) and filling factor (fraction of unit cell occupied by the pillar) are increased.

The proposed approach is particularly useful for polycrystalline samples with surface roughness in the range of tens of nanometers, which prevent us from measuring the dimensions precisely. Nevertheless, as the uncertainty is significantly smaller than the wavelength of light, effective optical dimensions can be defined that are further used for the simulation. These effective dimensions can then be finely tuned even when the uncertainty of the measurement is higher than the demanded thickness of the tuning layer.

For the experimental realization, we used a PhC slab with a thin waveguiding layer fabricated in a NCD layer via a combination of EBL and RIE. The SEM morphology of the PhC slab is shown in Figure 3(a). The dimensions of the PhC slabs, which were measured by reflectance interferometry (total thickness and thickness after etching) and determined from SEM images (column diameter and lattice constant), are shown in the table in Figure 1. The angle-resolved transmission measurement that reveals the spectral position of the leaky modes along the $\Gamma$–$X$ direction is shown in Figure 3(b). The spectral positions of the $TE_0$ and $TM_0$ leaky modes at normal incidence are $622 \pm 8$ and $582 \pm 5$ nm (where the FWHM of the dip is used as the uncertainty), respectively, which are well below the SiV center spectral line (738 nm).

The angular and spectral distribution of the leaky modes is directly mirrored into the extraction of the PL from the photonic crystals. Figure 3(e) shows the PL signal collected from the PhC slab (black lines) and from the planar reference layer surrounding the PhC slab (red lines) with objectives having NA from 0.12 to 0.90. The PL of the reference is spectrally broad due to the presence of intrinsic defects in NCD [45, 46] and it is extracted from guided modes solely via scattering on the diamond grains. The broad PL enables us to investigate coupling of the emission into a number of leaky modes for the case of the PhC. Leaky modes are clearly manifested in the PL spectra of the PhC measured with the NA 0.12 objective as two peaks superimposed on the broad PL background. When increasing the NA, the PL emission extracted via the leaky modes is summed up into the measured shape of the spectra. For the original PhC crystal, the extracted PL is located primarily below 700 nm.

The goal of the proposed approach was to spectrally shift the leaky modes so that the emission of the SiV centers overlaps with both the $TE_0$ and $TM_0$ modes located close to the $\Gamma$-point (i.e., extracted close to the vertical direction) in order to compare the coupling efficiency into the $TE_0$ and $TM_0$ modes. The thickness of the tuning layer necessary to achieve such a spectral shift of the modes was estimated to be ≈58 nm based on the RCWA simulation. Note that the original simulation parameters were modified to be in accordance with the measured parameters specified in the table in Figure 1.

We then performed the second diamond deposition, resulting in the PhC slab shown in Figure 3(c). Again, the PhC slab parameters are summarized in the table in Figure 1. The thickness of the tuning layer was ≈60 nm. The difference of 2 nm from the computed value is negligible with respect to the aim of this study. The diameter of the columns was

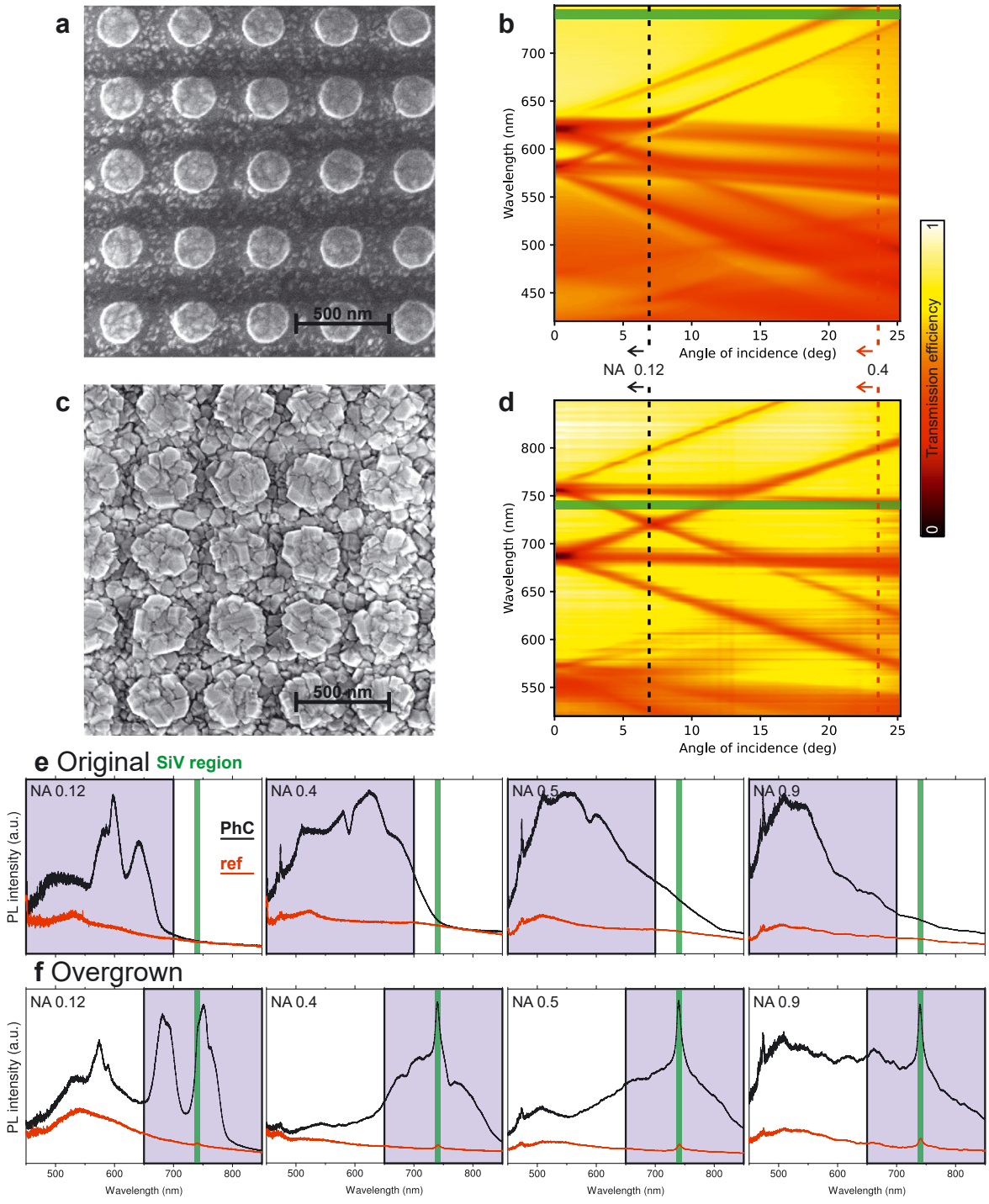


**Figure 3:** Scanning electron microscopy (SEM) images and measured transmission spectra (along Γ–*X* direction) of the original sample (a, b) and the sample after deposition of the tuning layer (c, d). (e) Photoluminescence (PL) spectra measured on the original structure (black on photonic crystal [PhC], red on reference layer; the green rectangle shows the spectral position of the SiV center zero-phonon line [ZPL]). (f) PL spectra measured on the structure with the tuning layer.

extended by ≈120 nm, which corresponds well with isotropic diamond growth. Note that after the deposition of the tuning layer, the shape of the columns is not perfectly cylindrical, as evidenced by the SEM images (Figure 3(c)). The surface roughness is higher after the deposition of the tuning layer, which is caused by the different diamond deposition systems

used. Nevertheless, the size of the grains is much smaller than the wavelength of the light and it does not disrupt the extraction via leaky modes. The increased roughness only enhances the nondirectional scattering of light from guided/leaky modes both on the PhC and the reference layer.

Figure 3(d) shows the angle-resolved transmission spectra of the PhC slab with the tuning layer measured along the Γ–$X$ direction. The spectral positions of the $TE_0$ and $TM_0$ leaky modes at normal incidence are 757 ± 6 and 688 ± 8 nm, respectively, and the spectral region at ≈738 nm now overlaps with the branches of both the $TE_0$ and $TM_0$ modes as desired. The overall red shift of the leaky modes due to the increased propagation constant is also reflected in the measured PL spectra of the PhC slab shown in Figure 3(f). The creation of SiV centers in the layer is evidenced by the ZPL emission of the SiV centers at ≈738 nm and is visible in all of the measured PL spectra of the planar reference. For the objective of NA 0.12 and the PhC slab, the SiV ZPL is hidden in the peak originating from the extraction via the vertical $TE_0$ mode. In contrast, the ZPL peak becomes dominant in the PL spectra measured with the objectives having NA>0.4, as explained in further detail below.

For precise evaluation of the PhC effect on the PL intensity, we define an enhancement factor as the ratio between the intensity measured on the PhC $I_{\mathrm{col}}^{\mathrm{PhC}}$ and the intensity measured on the unpatterned reference layer $I_{\mathrm{col}}^{\mathrm{ref}}$:

$$\mathrm{EF}(\lambda,\ \mathrm{NA}) = \frac{I_{\mathrm{col}}^{\mathrm{PhC}}(\lambda, NA)}{I_{\mathrm{col}}^{\mathrm{ref}}(\lambda, NA)}. \tag{3}$$

This enhancement factor depends on the wavelength and the objective used based on its NA. It is important to note that the enhancement factor represents the overall increase in intensity, which is not caused purely by the extraction of light via leaky modes. Firstly, the amount of light coupled to the radiative/guided modes depends on the slab thickness due to Fabry–Pérot (FP) resonances [47] that affect the emission intensity from both the PhC and the reference layer. Secondly, the volume of material and the surface area differ for the as-deposited diamond layer and the layer with the PhC slab. Note that the thickness of the reference layer is similar to the total thickness of the structure ($t_w + t_{\mathrm{PhC}}$) and thus the volume of the material is larger in the reference layer. Thirdly, the emitters at the top of the columns have a low probability of coupling to leaky modes, as the field of the modes is weak in these places (see Supplementary material) and they are preferentially emitted into free space in a diffuse (non-directional) manner. Fourthly, the scattering of light on NCD grains contributes to the extraction of light. Nevertheless, it contributes to the extraction for both the PhC structure and the reference layer and thus effectively decreases the observed enhancement with respect to a perfectly smooth layer. In addition to these photonic effects, the material itself can be altered during the fabrication process, which may lead to an increased number of defects that increase the absorption coefficient or the creation of new PL centers. Despite these effects, the enhancement factor representation is the most suitable for all applications, where the overall intensity is of importance (e.g., sensing or quantum light sources).

The enhancement factors for the original PhC slab and the PhC slab with the tuning layer are shown in Figure 4(a) and (b), respectively, and compared with the RCWA simulation of their transmission efficiency in the Γ–$X$ direction. The effect of extraction via leaky modes is clearly visible for a low NA 0.12 objective, where only the light extracted into the vicinity of the vertical direction is collected. For higher NA objectives, the enhancement is distributed over a broader spectral range as spectrally shifted leaky modes extracted into more inclined directions are also collected. Benefiting from the deposition of the tuning layer, the leaky modes in Figure 4(b) are red shifted onto the spectral region of the SiV centers, which significantly improves the enhancement in this region. The highest enhancement factor reaches ≈9 for NA 0.4 and 0.5 objectives. The effect of other factors (FP resonances, different volumes and surfaces and scattering) is very small, as evidenced by an only very small enhancement observed with the NA 0.12 objective in the regions where no leaky modes contribute to the extraction. Note that we have not used the resonant in-coupling of the excitation beam into the PhC slab as in [11].

Three spectral regions can be found in the enhancement spectra. In the first region (I in Figure 4), the enhancement factor grows with the NA of the objective used, as the number of modes contributing to the measured enhancement factor grows when higher collection angles are used. In the second region (II), the modes are located mainly in the vicinity of the vertical direction and the enhancement is high for the low NA 0.12 objective. In the third region (III), no leaky modes are located near the vertical direction and thus the enhancement is only measured with the high NA (>0.4) objectives. The dispersion of modes for other directions than Γ–$X$ that also contribute to the extraction of PL is shown in the Supplementary material for selected wavelengths.

The highest enhancement was observed at the spectral position of the SiV peak for all objectives except for NA 0.12, where the maximum enhancement is slightly red shifted. For other objectives, the enhancement of the SiV center spectral line is higher than in the neighboring spectral regions due to the different spatial distribution of SiV centers with regard to the PL defects forming the continuous PL background. The SiV centers are located primarily near the surface in the

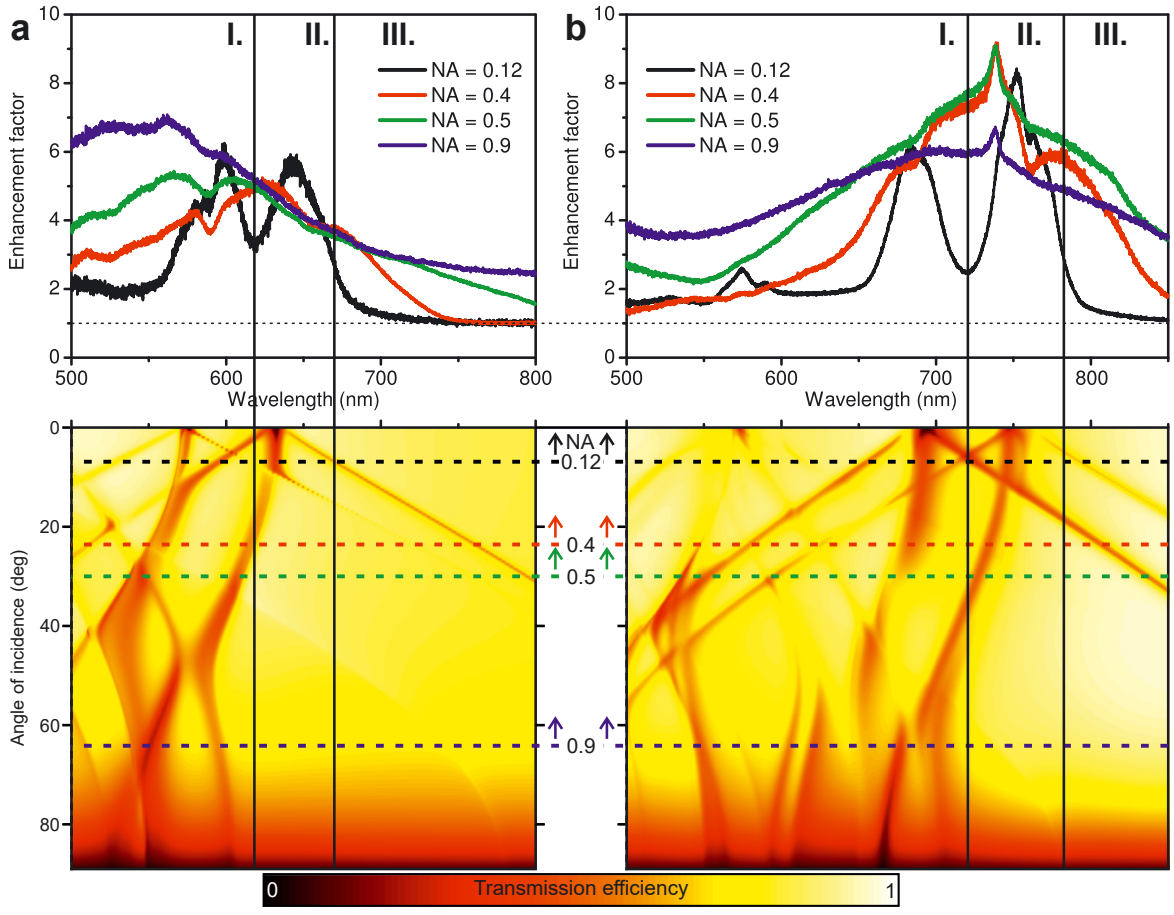


**Figure 4:** Top: Photoluminescence (PL) enhancement factor observed with microscope objectives with various numerical apertures (NAs) (a) before and (b) after the deposition of the tuning layer on the Photonic crystal (PhC) slab. Bottom: Simulated transmission spectra of the PhC slabs along the Γ–*X* direction for the corresponding spectral region. The horizontal dashed lines denote the maximum collection angle of the objective with specified NA. Vertical lines divide the spectra into three spectral regions that are discussed in the text.

tuning layer with ≈60 nm thickness. The emitters located at the very top of the columns therefore have a low probability of coupling to leaky/guided modes, which is a significant difference from the reference layer (see Supplementary material for a comparison of modal field distribution with the distribution of SiV centers). The light from these emitters is then radiated directly into the air. In contrast, the location of the SiV peak between the $TE_0$ and $TM_0$ modes allows both these modes to contribute to the extraction of the SiV peak when objectives with higher NA are used.

In order to compare the distribution of the SiV ZPL intensity between the $TE_0$ and $TM_0$ leaky modes, the angular dependence of emitted light was measured using the optical fiber for the collection of the PL providing an angular resolution of 1°. The measured dispersion of the modes (Figure 5(a)) corresponds to the angle-resolved transmission measurement (Figure 3(d)). Figure 5(a) shows that the light emitted by the SiV centers is more efficiently extracted via the $TE_0$ mode than the $TM_0$ mode. Employing the RCWA simulation, we computed that the fraction of energy localized in the tuning layer with SiV centers is 29.3% for the $TE_0$ mode, which is higher than 24% for the $TM_0$ mode. See Supplementary material for the simulated distribution of the electric field in the modes. This means that the coupling efficiency of the SiV PL to the $TE_0$ mode is 1.22 times higher than the coupling efficiency into the $TM_0$ mode, which agrees well with the observed ratio of the PL intensity between these modes (≈1.21). The outcoupling efficiency of the modes from the layer is similar for both modes, as evidenced by their similar linewidths in Figures 3(d) and 5. On the other hand, the $TM_0$ mode has a higher fraction of energy propagating in the air compared to the $TE_0$ mode (32.2% compared to 24.7%) and is thus more suitable for detecting changes in the refractive index in the surrounding environment.

As a final step, we performed an oxygen plasma treatment of the sample, which leads to oxygen termination of

the surface and improves the PL intensity of the SiV centers located near the diamond surface [9]. The increased intensity of SiV centers after the oxidation process is shown in Figure 5(b) and is also clearly seen for the flat-band of the $TE_0$ mode. The coupling of light emitted by SiV centers into the flat-band can be also used for sensing applications. The angle, into which the light at a given wavelength (e.g., SiV center ZPL) is extracted, is very sensitive to changes in the refractive index and the angular shift of this leaky mode could be used for the detection instead of the spectral shift. Note that the refractive index change after oxygen plasma treatment is negligible and does not affect the spectral position of the modes.

The resolution/accuracy of the presented approach depends on the adjustability of the diamond growth rate in the used deposition system. With the CVD systems that use silane as the source of Si, the shift of <0.5 nm per minute can be achieved, which makes this approach comparable with the oxidation method shown in Ref. [27]. The main advantage here is that the properties (e.g. SiV concentration or $sp^2$ phase content) of the tuning layer can be controlled. Moreover, these methods are complementary as the oxidation process enable blue shift of the photonic modes, while our approach leads to the red shift of the modes. With the gas condensation technique, red shift of 0.07 nm per step was achieved for nanobeam cavities [37], which is beyond the reach of our approach, even when very slow growth rate and short deposition time are used. However, such tuning can be done only inside the cryostat chamber and it is not permanent, and it is thus not suitable for many applications (e.g. sensing). The spectral range of the gas tuning method is also limited in comparison to our method.

The tuning of photonic modes by the presented approach could be also employed for single-crystal diamond-based photonic structures, e.g., PhC cavities, nanobeam cavities, or nanopillars. Similarly to the photonic structures in NCD, the dimensions of these structures usually deviate from the optimal dimensions designed by numerical simulations. The spectral position of the photonic modes of these structures depends strongly on their dimensions and can thus be shifted by the deposition of a thin tuning layer.

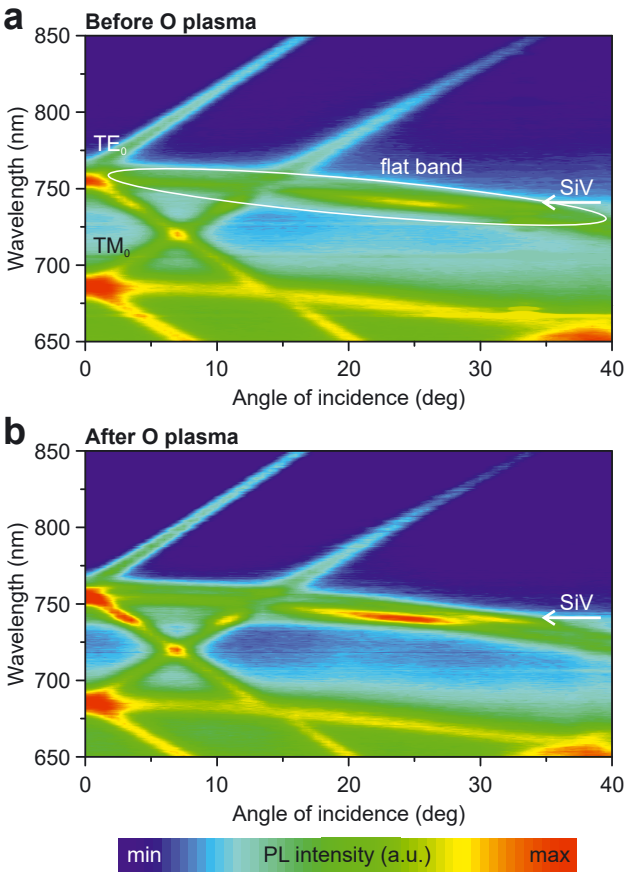


**Figure 5:** Angle-resolved photoluminescence (PL) along the Γ–*X* direction (a) before and (b) after the oxygen plasma treatment.

## 4 Conclusion

In summary, we have shown using computer simulation that control over the spectral position of leaky modes in 2D PhC slabs requires knowledge of the material parameters and nanometer scale precision of the fabrication process, which is often beyond the fabrication possibilities. Therefore, we have proposed and demonstrated a fabrication approach based on the deposition of a tuning layer onto a precharacterized PhC slab with intentionally blue-shifted leaky modes that enables us to spectrally shift the photonic modes to the required spectral position. We were able to shift the photonic modes of the 2D PhC slabs by more than 100 nm to the spectral position of SiV centers in diamond and achieved ninefold enhancement of the SiV center emission line without resonant excitation of the sample. Simultaneously, the tuning layer contained optically active SiV centers, the presence of which near the diamond surface is favorable for detection of changes in the surrounding environment. The proposed method may contribute to the cost-effective fabrication of 2D PhC slabs for applications in sensorics, where the initial PhC slab may be fabricated using large-scale methods, such as nanoimprint or nanosphere lithography. The method can also be adapted to tune the position of modes of other photonic structures in diamond, such as nanopillars, photonic crystal cavities or nanobeam cavities, which are of very high interest in the fields of quantum optics, quantum information processing and

sensing applications. Finally, the proposed method can also be extended towards other optical centers in diamond suitable for detection, such as NV centers.

**Author contributions:** All the authors have accepted responsibility for the entire content of this submitted manuscript and approved submission.

**Research funding:** This work was supported by the grant GACR 19-14523S, by the Lumina project of the Czech Academy of Sciences, and the Operational Programme Research, Development and Education financed by European Structural and Investment Funds (ERDF) and the Czech Ministry of Education, Youth and Sports (MEYS) project CZ.02.1.01/0.0/0.0/16_019/0000760 (SOLID21). B. Rezek also acknowledges support from the ERDF and MEYS project CZ.02.1.01/0.0/15_003/0000464 (CAP).

**Conflict of interest statement:** The authors declare no conflicts of interest regarding this article.

## References

[1] I. Aharonovich, A. D. Greentree, and S. Prawer, "Diamond photonics," *Nat. Photonics*, vol. 5, pp. 397–405, 2011.

[2] I. Aharonovich, S. Castelletto, D. A. Simpson, C.-H. Su, A. D. Greentree, and S. Prawer, "Diamond-based single-photon emitters," *Rep. Prog. Phys.*, vol. 74, p. 076501, 2011.

[3] T. Schröder, S. L. Mouradian, J. Zheng, et al., "Quantum nanophotonics in diamond [Invited]," *J. Opt. Soc. Am. B*, vol. 33, pp. B65–B83, 2016.

[4] S. Hong, M. S. Grinolds, L. M. Pham, et al., "Nanoscale magnetometry with NV centers in diamond," *MRS Bull.*, vol. 38, pp. 155–161, 2013.

[5] L. Rondin, J.-P. Tetienne, T. Hingant, J.-F. Roch, P. Maletinsky, and V. Jacques, "Magnetometry with nitrogen-vacancy defects in diamond," *Rep. Prog. Phys.*, vol. 77, p. 056503, 2014.

[6] C. Blin, Z. Han, H. A. Girard, et al., "Surface-sensitive diamond photonic crystals for high-performance gas detection," *Opt. Lett.*, vol. 41, pp. 4360–4363, 2016.

[7] E. Bernardi, R. Nelz, S. Sonusen, and E. Neu, "Nanoscale sensing using point defects in single-crystal diamond: recent progress on nitrogen vacancy center-based sensors," *Crystals*, vol. 7, p. 124, 2017.

[8] E. Neu, D. Steinmetz, J. Riedrich-Möller, et al., "Single photon emission from silicon-vacancy colour centres in chemical vapour deposition nano-diamonds on iridium," *New J. Phys.*, vol. 13, p. 025012, 2011.

[9] S. Stehlik, L. Ondic, M. Varga, et al., "Silicon-vacancy centers in ultra-thin nanocrystalline diamond films," *Micromachines*, vol. 9, p. 281, 2018.

[10] L. Ondič, M. Varga, K. Hruška, J. Fait, and P. Kapusta, "Enhanced extraction of silicon-vacancy centers light emission using bottom-up engineered polycrystalline diamond photonic crystal slabs," *ACS Nano*, vol. 11, pp. 2972–2981, 2017.

[11] J. Fait, M. Varga, K. Hruška, et al., "Maximized vertical photoluminescence from optical material with losses employing resonant excitation and extraction of photonic crystal modes," *Nanophotonics*, vol. 8, pp. 1041–1050, 2019.

[12] J. Wolters, A. W. Schell, G. Kewes, et al., "Enhancement of the zero phonon line emission from a single nitrogen vacancy center in a nanodiamond via coupling to a photonic crystal cavity," *Appl. Phys. Lett.*, vol. 97, p. 141108, 2010.

[13] J. Riedrich-Möller, C. Arend, C. Pauly, et al., "Deterministic coupling of a single silicon-vacancy color center to a photonic crystal cavity in diamond," *Nano Lett.*, vol. 14, pp. 5281–5287, 2014.

[14] L. Ondič, M. Varga, J. Fait, et al., "Photonic crystal cavity-enhanced emission from silicon vacancy centers in polycrystalline diamond achieved without postfabrication fine-tuning," *Nanoscale*, vol. 12, pp. 13055–13063, 2020.

[15] A. Faraon, P. E. Barclay, C. Santori, K.-M. C. Fu, and R. G. Beausoleil, "Resonant enhancement of the zero-phonon emission from a colour centre in a diamond cavity," *Nat. Photonics*, vol. 5, pp. 301–305, 2011.

[16] E. Purcell, "Spontaneous emission probabilities at radio frequencies," *Phys. Rev.*, vol. 69, p. 681, 1946.

[17] K. Srinivasan and O. Painter, "Momentum space design of high-Q photonic crystal optical cavities," *Opt. Express*, vol. 10, pp. 670–684, 2002.

[18] J. Vuckovic, M. Loncar, H. Mabuchi, and A. Scherer, "Optimization of the Q factor in photonic crystal microcavities," *IEEE J. Quant. Electron.*, vol. 38, pp. 850–856, 2002.

[19] T. Nakamura, Y. Takahashi, Y. Tanaka, T. Asano, and S. Noda, "Improvement in the quality factors for photonic crystal nanocavities via visualization of the leaky components," *Opt. Express*, vol. 24, pp. 9541–9549, 2016.

[20] C. Blin, X. Checoury, H. A. Girard, et al., "Optical analysis of p-type surface conductivity in diamond with slotted photonic crystals," *Adv. Opt. Mater.*, vol. 1, pp. 963–970, 2013.

[21] C. Becker, P. Wyss, D. Eisenhauer, et al., "$5 \times 5$ cm$^2$ silicon photonic crystal slabs on glass and plastic foil exhibiting broadband absorption and high-intensity near-fields," *Sci. Rep.*, vol. 4, 2014, https://doi.org/10.1038/srep05886.

[22] S. Fan and J. D. Joannopoulos, "Analysis of guided resonances in photonic crystal slabs," *Phys. Rev. B*, vol. 65, p. 235112, 2002.

[23] G. Pitruzzello and T. F. Krauss, "Photonic crystal resonances for sensing and imaging," *J. Opt.*, vol. 20, p. 073004, 2018.

[24] W. Chen, K. D. Long, M. Lu, et al., "Photonic crystal enhanced microscopy for imaging of live cell adhesion," *Analyst*, vol. 138, pp. 5886–5894, 2013.

[25] A. Kromka, O. Babchenko, Š. Potocký, B. Rezek, and A. Sveshnikov, "Diamond nucleation and seeding techniques for tissue regeneration," in *Diamond-Based Materials for Biomedical Applications*, Cambridge, Woodhead Publishing, 2013, pp. 206–255.

[26] Š. Potocký, T. Ižák, M. Varga, and A. Kromka, "Influence of gas chemistry on Si-V color centers in diamond films," *Phys. Status Solidi B*, vol. 252, pp. 2580–2584, n.d.

[27] J. Riedrich-Möller, L. Kipfstuhl, C. Hepp, et al., "One- and two-dimensional photonic crystal microcavities in single crystal diamond," *Nat. Nanotechnol.*, vol. 7, pp. 69–74, 2012.

[28] S. Kim, J. E. Fröch, J. Christian, et al., "Photonic crystal cavities from hexagonal boron nitride," *Nat. Commun.*, vol. 9, p. 2623, 2018.
[29] K. Hennessy, A. Badolato, A. Tamboli, et al., "Tuning photonic crystal nanocavity modes by wet chemical digital etching," *Appl. Phys. Lett.*, vol. 87, p. 021108, 2005.
[30] M. Clementi, A. Barone, T. Fromherz, D. Gerace, and M. Galli, "Selective tuning of optical modes in a silicon comb-like photonic crystal cavity," *Nanophotonics*, vol. 9, pp. 205–210, 2020.
[31] S. Vignolini, F. Riboli, F. Intonti, et al., "Mode hybridization in photonic crystal molecules," *Appl. Phys. Lett.*, vol. 97, p. 063101, 2010.
[32] M. A. Dündar, J. A. M. Voorbraak, R. Nötzel, A. Fiore, and R. W. van der Heijden, "Multimodal strong coupling of photonic crystal cavities of dissimilar size," *Appl. Phys. Lett.*, vol. 100, p. 081107, 2012.
[33] A. C. Liapis, B. Gao, M. R. Siddiqui, Z. Shi, and R. W. Boyd, "On-chip spectroscopy with thermally tuned high-Q photonic crystal cavities," *Appl. Phys. Lett.*, vol. 108, p. 021105, 2016.
[34] T. Cai, R. Bose, G. S. Solomon, and E. Waks, "Controlled coupling of photonic crystal cavities using photochromic tuning," *Appl. Phys. Lett.*, vol. 102, p. 141118, 2013.
[35] pi D. Sridharan, R. Bose, H. Kim, G. S. Solomon, and E. Waks, "A reversibly tunable photonic crystal nanocavity laser using photochromic thin film," *Opt. Express*, vol. 19, pp. 5551–5558, 2011.
[36] J. L. Zhang, S. Sun, M. J. Burek, et al., "Strongly cavity-enhanced spontaneous emission from silicon-vacancy centers in diamond," *Nano Lett.*, vol. 18, pp. 1360–1365, 2018.
[37] J. C. Lee, D. O. Bracher, S. Cui, et al., "Deterministic coupling of delta-doped nitrogen vacancy centers to a nanobeam photonic crystal cavity," *Appl. Phys. Lett.*, vol. 105, p. 261101, 2014.
[38] M. Varga, V. Vretenar, T. Izak, V. Skakalova, and A. Kromka, "Carbon nanotubes overgrown and ingrown with nanocrystalline diamond deposited by different CVD plasma systems," *Phys. Status Solidi B*, vol. 251, pp. 2413–2419, 2014.
[39] Š. Potocký, J. Holovský, Z. Remeš, M. Müller, J. Kočka, and A. Kromka, "Si-related color centers in nanocrystalline diamond thin films," *Phys. Status Solidi B*, vol. 251, pp. 2603–2606, 2014.
[40] K. Ohno, F. Joseph Heremans, L. C. Bassett, et al., "Engineering shallow spins in diamond with nitrogen delta-doping," *Appl. Phys. Lett.*, vol. 101, p. 082413, 2012.
[41] V. Sedov, V. Ralchenko, A. A. Khomich, et al., "Si-doped nano- and microcrystalline diamond films with controlled bright photoluminescence of silicon-vacancy color centers," *Diam. Relat. Mater.*, vol. 56, pp. 23–28, 2015.
[42] V. Haerle, B. Hahn, S. Kaiser, et al., "High brightness LEDs for general lighting applications using the new ThinGaN™-technology," *Phys. Status Solidi A*, vol. 201, pp. 2736–2739, 2004.
[43] T. Fujii, Y. Gao, R. Sharma, E. L. Hu, S. P. DenBaars, and S. Nakamura, "Increase in the extraction efficiency of GaN-based light-emitting diodes via surface roughening," *Appl. Phys. Lett.*, vol. 84, pp. 855–857, 2004.
[44] M. Hammer, *1-D Multilayer Slab Waveguide Mode Solver*, 2020. Available at: https://www.computational-photonics.eu/oms.html.
[45] L. Bergman, M. T. McClure, J. T. Glass, and R. J. Nemanich, "The origin of the broadband luminescence and the effect of nitrogen doping on the optical properties of diamond films," *J. Appl. Phys.*, vol. 76, pp. 3020–3027, 1994.
[46] P. Galář, B. Dzurňák, M. Varga, M. Marton, A. Kromka, and P. Malý, "Influence of non-diamond carbon phase on recombination mechanisms of photoexcited charge carriers in microcrystalline and nanocrystalline diamond studied by time resolved photoluminescence spectroscopy," *Opt. Mater. Express*, vol. 4, pp. 624–637, 2014.
[47] H. Benisty, H. D. Neve, and C. Weisbuch, "Impact of planar microcavity effects on light extraction – part I: basic concepts and analytical trends," *IEEE J. Quant. Electron.*, vol. 34, pp. 1612–1631, 1998.

**Supplementary Material:** The online version of this article offers supplementary material (https://doi.org/10.1515/nanoph-2021-0369).